AGU PUBLICATIONS

JGR

Journal of Geophysical Research: Space Physics

RESEARCH ARTICLE
10.1002/2014JA020926

Key Points:
- Analysis of the dynamics of high-velocity comet clumps
- Analyze the clump interaction with the solar wind
- Discuss the origin and composition of the clumps

Supporting Information:
- Text S1
- Movie S1

Correspondence to:
N.-E. Raouafi,
NourEddine.Raouafi@jhuapl.edu

Citation:
Raouafi, N.-E., C. M. Lisse, G. Stenborg, G. H. Jones, and C. A. Schmidt (2015), Dynamics of HVECs emitted from comet C/2011 L4 as observed by STEREO, *J. Geophys. Res. Space Physics*, *120*, 5329–5340, doi:10.1002/2014JA020926.

Received 1 JAN 2015
Accepted 29 JUN 2015
Accepted article online 4 JUL 2015
Published online 29 JUL 2015

Dynamics of HVECs emitted from comet C/2011 L4 as observed by STEREO

N.-E. Raouafi[1], C. M. Lisse[1], G. Stenborg[2], G. H. Jones[3], and C. A. Schmidt[4]

[1]The Johns Hopkins University Applied Physics Laboratory, Laurel, Maryland, USA, [2]SPACS, College of Science, George Mason University, Fairfax, Virginia, USA, [3]Mullard Space Science Laboratory, UCL, Dorking, UK, [4]Materials Science and Engineering, University of Virginia, Charlottesville, Virginia, USA

Abstract High-quality white-light images from the Sun-Earth Connection Coronal and Heliospheric Investigation (SECCHI) HI-1 telescope on board STEREO-B reveal high-velocity evanescent clumps (HVECs) expelled from the coma of the C/2011 L4 (Pan-STARRS) comet. The observations were recorded around the comet's perihelion (i.e., ~0.3 AU) during the period 9–16 March 2013. Animated images provide evidence of highly dynamic ejecta moving near radially in the antisunward direction. The bulk speed of the clumps at their initial detection in the HI1-B images range from 200 to 400 km s^{-1} followed by an appreciable acceleration up to speeds of 450–600 km s^{-1}, which are typical of slow to intermediate solar wind speeds. The clump velocities do not exceed these limiting values and seem to reach a plateau. The images also show that the clumps do not expand as they propagate. The white-light images do not provide direct insight into the composition of the expelled clumps, which could potentially be composed of fine, submicron dust particles, neutral atoms and molecules, and/or ionized atomic/molecular cometary species. Although solar radiation pressure plays a role in accelerating and size sorting of small dust grains, it cannot accelerate them to velocities >200 km s^{-1} in the observed time interval of a few hours and distance of $<10^6$ km. Further, order of magnitude calculations show that ionized single atoms or molecules accelerate too quickly compared to observations, while dust grains micron sized or larger accelerate too slowly. We find that neutral Na, Li, K, or Ca atoms with $\beta > 50$ could possibly fit the observations. Just as likely, we find that an interaction with the solar wind and the heliospheric magnetic field can cause the observed clump dynamical evolution, accelerating them quickly up to solar wind velocities. We thus speculate that the HVECs are composed of charged particles (dust particles) or neutral atoms accelerated by radiation pressure at $\beta > 50$ values. In addition, the data suggest that clump ejecta initially move along near-radial, bright structures, which then separate into HVECs and larger dust grains that steadily bend backward relative to the comet's orbital motion due to the effects of solar radiation and gravity. These structures gradually form new striae in the dust tail. The near-periodic spacing of the striae may be indicative of outgassing activity modulation due to the comet nucleus' rotation. It is, however, unclear whether all striae are formed as a result of this process.

1. Introduction

Although comets have been observed for centuries, phenomena related to their morphologies; composition; formation of neutral, ion, and dust tails; and interaction with the local environment (e.g., solar wind) are still not completely understood. Observations show that cometary nuclei, which are composed of dusty ices (i.e., water and other volatile ices, such as CO and CO_2), have fragile structures that are susceptible to heat-driven fragmentation (e.g., shedding or sloughing, fission or shattering, and disintegration) [see *Clark et al.*, 2004], sublimation, evaporation, and photoionization of diverse molecular species such as H_2O, CO, N_2, CO_2, OH, CN, CH, NH, C_3, and NH_2 [*Brandt*, 1968; *Lee et al.*, 2014].

Early ground-based observations of comets led to the conclusion that cometary activity must originate from discrete locations on the nuclei surfaces. This was based on the diverse morphologies within cometary comas such as jets, expanding halos, and fan-shaped comas. These are thought to be the result of the combined effects of the localized activity on the nuclei surfaces and their rotation as well as their Sun-comet (seasonal variations) and Earth-comet geometries [see *Sekanina*, 2007, and references therein]. Close-up images of comet nuclei from flyby space missions (e.g., Giotto: comets Halley and Grigg-Skjellerup

[*Keller et al.*, 1986, 1987]; Deep Space 1: comet 19P/Borrelly [*Soderblom et al.*, 2002a, 2002b]; Stardust: comet 81P/Wild [*Brownlee et al.*, 2004]; Deep Impact: comet Tempel 1 [*A'Hearn et al.*, 2005]; and Rosetta: comet 67P/Churyumov-Gerasimenko [*Glassmeier et al.*, 2007]) could only confirm this conclusion [*Brownlee et al.*, 2004; *Sekanina et al.*, 2004]. They particularly show that most of the nuclei surfaces are dark, inert, inactive, and refractory. The heat-driven activity of the cometary nuclei is contained in isolated bright sites on the surface or from subsurface cavities [*Yelle et al.*, 2004] where gases escape mostly sunward in the form of jets carrying with them chunks of ice-mixed dust as proposed by *Whipple* [1951] in his conglomerate model [see also *Clark et al.*, 2004].

Dust tail striae are thought to form through the fragmentation of dust agglomerates [*Sekanina and Farrell*, 1980, 1982; *Hill and Mendis*, 1980; *Notni and Thaenert*, 1988; *Nishioka and Watanabe*, 1990; *Pittichová et al.*, 1997]. The escaping gases drag ice-mixed dust forming a strongly coupled ensemble in the vicinity of the nucleus, which then decouple as they expand farther out leaving the several hundreds of m s^{-1} fast icy conglomerates exposed to the solar conditions (solar heat, electrostatic charging, collisions, etc.) [see *Konno et al.*, 1990; *Clark et al.*, 2004]. The exposure of the ejected material leads to further sublimation of the ices, which causes further fragmentation of bare, porous, and fragile dust aggregates. Radiation pressure forces gradually modify the dust and gas trajectories antisunward and then into the different tails (i.e., dust, ion, and neutral tails). Another discovery from the Stardust mission supporting the theories of dust aggregate fragmentation was reported by *Tuzzolino et al.* [2004]. They found strong fluctuations in particle number density in 100 ms or less corresponding to distances $\ll$ 1 km, which at times were intercepted by gaps with very low to practically no particles [see also *Clark et al.*, 2004]. For a review on the dynamics of cometary comas, see *Sekanina* [2007].

The pickup of the ionized species by the solar wind and the embedded heliospheric magnetic field (HMF) results in the formation of the plasma (or ion) tail, which is susceptible to electromagnetic forces of the ambient environment and changes in the solar wind conditions. The plasma tail is hence swept antisunward with a velocity-aberration correction of a few degrees depending on the comet's speed relative to that of the solar wind [*Ershkovich*, 1976; *Mendis et al.*, 1986; *Russell et al.*, 1982; *Farnham and Meech*, 1994; *Jones et al.*, 2004; *Buffington et al.*, 2008; *Clover et al.*, 2010; *Jackson et al.*, 2013]. Along with the volatile species, dust particles with different sizes lift off from the nucleus surface into the cometary coma where they become exposed to an array of physical processes (e.g., gravity, radiation pressure, fragmentation, charging, and collisions) [*Konno et al.*, 1993; *Kimura et al.*, 2002; *Mendis and Horányi*, 2013], dictating their subsequent dynamical evolution.

Large dust particles (i.e., $>$ 1 μm) are typically dominated by the effects of solar gravity and radiation pressure forces and form a rather morphologically diffuse tail. Thus, the dust tail, which is formed by particles that are individually in orbit around the Sun, varies from linear antisolar to curved along the orbit [*Lisse et al.*, 1998, 2004]. The range of ratios of solar gravity to solar radiation forces on these particles causes the size sorting as well as the dust tail morphology to curve as the comet swings around the Sun. The orbital motions of supramicron particles may only be affected by extreme solar wind events, such as coronal mass ejections (CMEs) [*Jones and Brandt*, 2004; *Jia et al.*, 2009]. Due to solar photon-driven photoelectric effect and solar wind sputtering, it is also expected that dust grains become charged and every low mass particle ($<$ 0.1 μm) becomes susceptible to the effects of the HMF and the solar wind [e.g., *Mendis and Horányi*, 1991; *Kramer et al.*, 2014].

C/2011 L4 (Panoramic Survey Telescope and Rapid Response System (Pan-STARRS); Figure 1), a nonperiodic comet, was discovered on 6 June 2011 at 7.9 AU heliocentric distance with an apparent magnitude of 19 [*Wainscoat et al.*, 2011]. It was first observed by the 1.8 m Pan-STARRS 1 survey telescope (Haleakala, HI) and later by the Canada-France-Hawaii Telescope (http://www.cfht.hawaii.edu). It became visible to the naked eye, with a visual magnitude of −1.0, near its perihelion at 0.3 AU in February–March 2013. It is one of the brightest comets since the great comet C/1995 O1 (Hale-Bopp) [*Yang et al.*, 2014]. Orbital analyses (Figure 2) indicate that it is likely a new comet from the Oort cloud [e.g., *Królikowska et al.*, 2012]. C/2011 L4 provide therefore a great opportunity to monitor the composition and dynamics of relatively pristine, unprocessed comets.

The dust and gas production of comet C/2011 L4 is enigmatic. The comet was more active before perihelion than after [*Combi et al.*, 2014]. C/2011 L4 is an unusually dust-rich comet with very low gas emission [*Fulle et al.*, 2013; *Yang et al.*, 2014]. The comet activity was first observed beyond the water-ice sublimation zone (i.e., 5–6 AU from the Sun) [*Yang et al.*, 2014]. This early activity may be explained by latent heat release from the amorphous-crystalline water-ice transition, sublimation of frozen supervolatiles, and/or comet fragmentation [*Prialnik*, 1992; *Notesco et al.*, 2003; *Bar-Nun and Laufer*, 2003; *Meech and Svoren*, 2004; *Boehnhardt*, 2004;

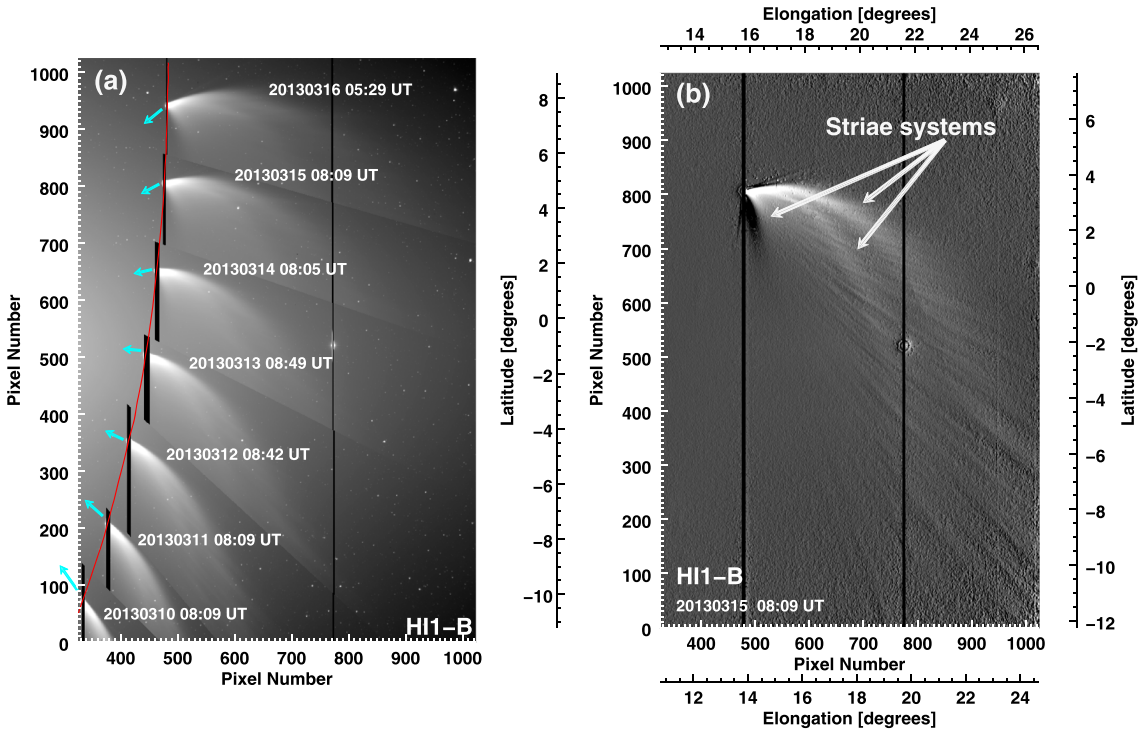

Figure 1. (a) Composite intensity images of STEREO/SECCHI/HI-1B showing different phases of the C/2011 L4 comet. The recording dates of the different images are indicated. The red curve shows the orbit of the comet, and the arrows point toward the Sun center. (b) Filtered image highlighting the rate of local intensity changes. The dust tail is particularly noticeable with at least three systems of striae, which are pointed to by arrows. The dark vertical lines are saturated pixel arrays due to CCD (i.e., charge-coupled device) bleeding.

Yang et al., 2014]. Spectral observations of C/2011 L4 showed strong emission in the 2.0 μm spectral band and a rather weak emission in the 1.5 μm band [*Yang et al.*, 2014]. *Yang et al.* [2014] showed through Mie modeling that the ratio between the depths of these spectral bands is sensitive to ice grain size. They particularly found that the inclusion of submicron grains allows the prominent 2.0 μm and the much weaker 1.5 μm bands to be reproduced fairly well. They argue that the comet spectra may be explained by ∼30% very fine grained (i.e., ∼0.2 μm) ice mixed with spectrally featureless materials and that the distant activity of C/2011 L4 could be driven by highly volatile ices such as CO_2.

C/2011 L4 was observed by the Sun-Earth Connection Coronal and Heliospheric Investigation (SECCHI) [*Howard et al.*, 2008] heliospheric imagers HI-1 and HI-2 [*Socker et al.*, 2000] on board the Solar Terrestrial Relations Observatory (STEREO) [*Kaiser et al.*, 2008] Behind (i.e., STEREO-B) on 9–16 March 2013. The high quality of the recorded images show evidence for abundant dust in the comet's coma and tail with rich dynamical structures, including multiple striae (Figure 1) as well as a series of unusual high-velocity evanescent clumps (hereafter HVECs) propagating antisunward (Figure 3).

The main aim of this work is the characterization the HVECs and their interaction with the local solar wind as well as their connection to newly formed striae in the dust tail based mainly on STEREO/HI-1B observations. The paper is organized as follows: observations and data processing are briefly described in section 2. Section 3 is dedicated to the data analysis. Discussion of the results and conclusions are given in section 4.

Although we speculate on the processes at the origin of the HVECs and physical mechanisms that may influence their dynamical behavior, rigorous modeling of dynamics of these features is out of the scope of this paper and is therefore left for a future publication.

2. Observations and Data Processing

The STEREO payload comprises two white-light imagers (termed HI-1 and HI-2 with respective spectral band passes of 630–730 nm and 400–1000 nm and near-flat quantum efficiency of the detectors of >90% within the wavelength range 500–700 nm) [see *Eyles et al.*, 2009]. They are dedicated to heliospheric observations

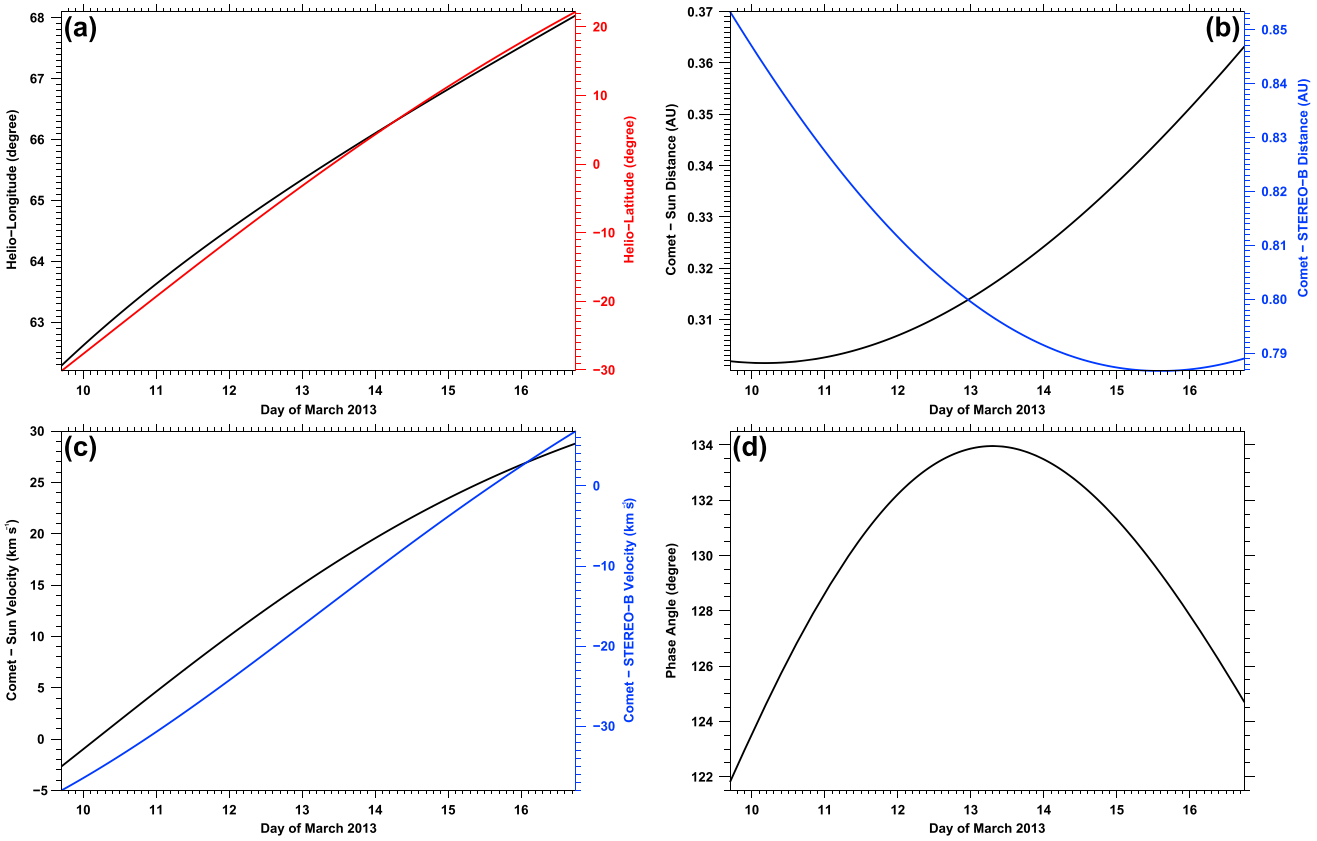

Figure 2. C/2011 L4 orbital parameters during the period of the crossing the field of view of STEREO/HI1-B. (a) Heliolongitude (black) and heliolatitude (red); (b) comet heliodistance (black) and distance to STEREO-B (blue); (c) velocity of the comet with respect to the Sun (black) and STEREO-B (blue). Negative (positive) velocities mean the comet is moving toward (away from) the Sun or STEREO-B. (d) Phase angle of the comet. Data source: http://ssd.jpl.nasa.gov/horizons.cgi.

with combined fields of view (FOVs) covering solar elongations ranging from 4.0° to 88.7°. The HI-1 and HI-2 optical axes are nominally set in the ecliptic plane at 14.0° and 53.7° from the Sun, with respective FOVs of 20° and 70°. The detectors are 2048 × 2048 arrays with 13.5 × 13.5 μm^2 pixel size. The onboard 2 × 2 binning results in respective image angular resolutions of ~105.0″ and ~6.0′. Details of the optical specifications and calibration of the HI-1 and HI-2 instruments are given by *Eyles et al.* [2009] and *Bewsher et al.* [2012].

C/2011 L4 crossed the HI-1B FOV between 9 March 2013 ~16:50 UT and 16 March 2013 ~18:00 UT (see Figure 1). Figure 2 provides the orbital parameters of the comet within the HI1-B FOV for the period 9–16 March 2013. The phase angle (Sun-C/2011 L4-STEREO-B) varied from ~122° to ~134°. This section of the comet orbit was mostly south-north oriented with a nearly constant speed of ~95 km s^{-1} as seen from STEREO-B (i.e., projected on the plane of the sky). With respect to the Sun, the comet's velocity varies from −2.7 km s^{-1} to 28.8 km s^{-1}. The comet reached its perihelion distance of ~0.301 AU on 10 March at 04:04 UT [*Combi et al.*, 2014]. As seen from STEREO-B, the comet's apparent closest distance to the Sun was ~49.0 $R_\odot$ (i.e., 0.23 AU) on 12 March at 18:50 UT. The extent of the dust tail, which was observed with an angle ~130° between the line of sight and the comet's orbit plane by both HI1-B and HI-2B, was greater than 10^7 km (~100 $R_\odot$). It remained visible in HI-1B and HI-2B FOVs until 19 and 22 March, respectively.

The present analysis is mainly based on white-light images recorded by STEREO/SECCHI/HI-1B during the period of 9–16 March 2013. The images are recorded with a cadence of 40 min. Images from HI-2 (not shown here) recorded with a cadence of 2 h were used for qualitative analysis. Level 0.5 data acquired from the Virtual Solar Observatory (VSO: http://www.virtualsolar.org) database are processed to higher levels using the instruments' calibration procedures available in the Solar Software tree (SSW: http://www.lmsal.com/solarsoft). The STEREO observations provide unprecedented details of the morphology of the dust tail, including multiple striae systems (see Figure 1b). A novel phenomenon of HVECs presumably ejected from the comet nucleus is also clearly noticeable in running-difference images as they propagate antisunward (see Figure 3).

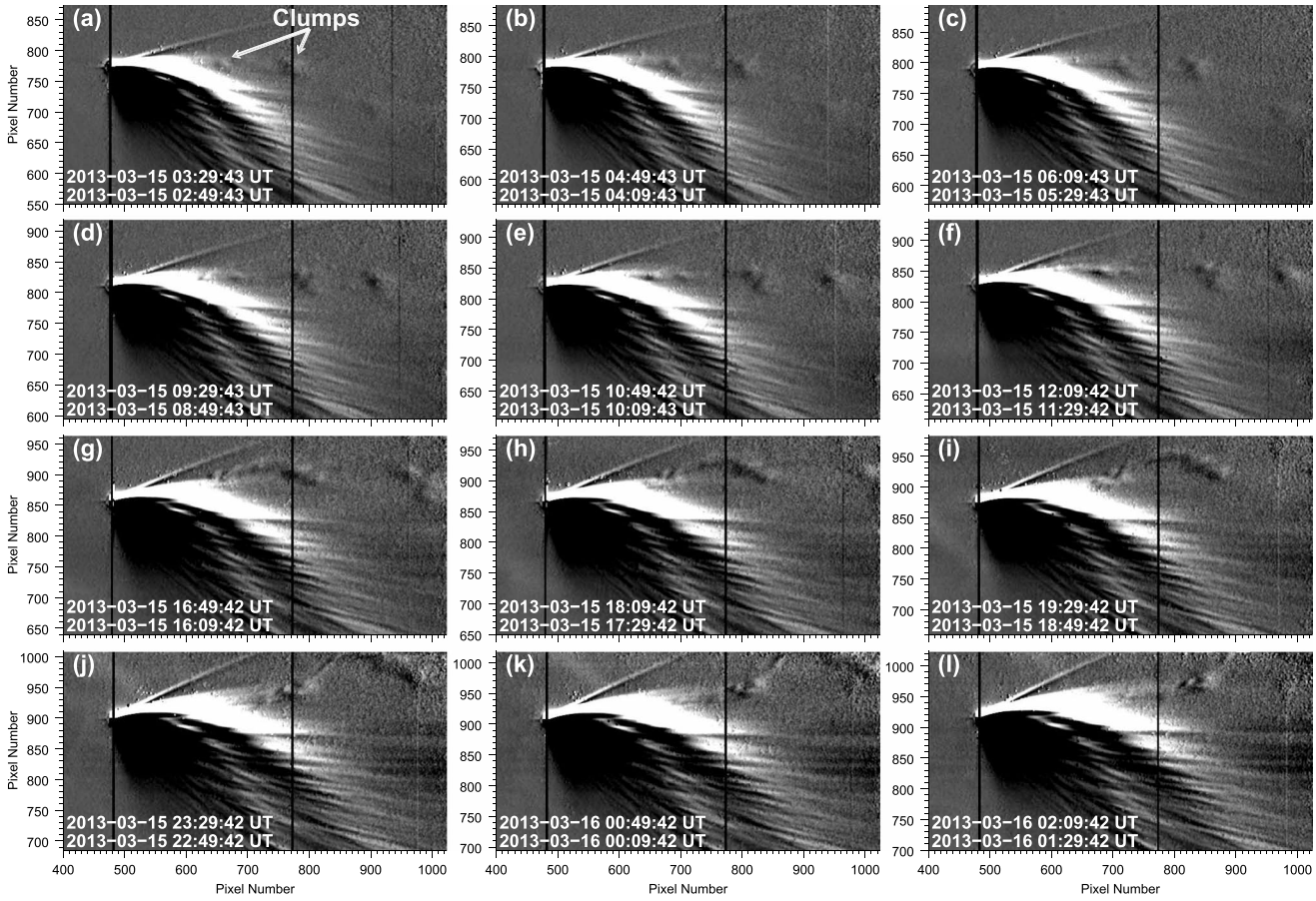

Figure 3. (a–l) STEREO/SECCHI/HI-1B running-difference images illustrating the HVECs ejected from the C/2011 L4 coma. The dates and times on each panel correspond to the image pair used for the running-difference images. The clumps are first detected at cometocentric distances ranging from $\sim 6 \times 10^6$ km to $\sim 10^7$ km ($\sim$0.041–0.076 AU; see Table1). The arrows in Figure 3a point to two clumps. The HVECs initially move along near-radial structures, which progressively bend backward to form new striae in the dust tail (see Figures 3g–3l and Movie S1 in the supporting information). The HVECs ejection and the quasiperiodicity of the striae may correspond to distinctive activity events on the comet surface (e.g., jets).

The focus in this work is on these transient bright clumps; we leave dynamical analysis of the comet's large dust particle tail to a future paper. Based on the images of HI1-B, we determine the clump's dynamical properties as well as their relationship with newly forming striae in the dust tail. The use of the SSW procedures alone was insufficient to analyze the bright clumps, and supplemental image processing was necessary. In particular, we used techniques such as homomorphic filtering [*Oppenheim et al.*, 1968], to simultaneously normalize the brightness and increase the contrast across the HI images and hence make clearer the faint transient features of interest and the fine structure within the dust tail. As implemented, the procedure helps remove the effects of sky background (i.e., light scattered off electrons and dust: *K* and *F* corona, respectively). The star field was minimized by applying a sigma filter available in the SSW. For example, compare the raw intensity image in Figure 1a and the processed image in Figure 1b.

3. Data Analysis

Table 1 lists 12 HVECs expelled from the C/2011 L4 coma. The dates and times of their appearance, the corresponding heliocentric and cometocentric distances, position angles, and dates and times of their disappearance are also shown. The sizes of these structures are determined using the running-difference images. The values shown in Table 1 are the averages of the measured size at different times, which do not change significantly. The size error is the standard deviation of the measurements divided by their numbers. The running-difference images displayed in Figure 3 illustrates several of the HVECs. A number of these clumps could also be traced within the HI-2B FOV, particularly the ones ejected northward of the ecliptic plane. It is, however, harder to characterize their propagation within HI-2B FOV because of the lower cadence and

Table 1. List of HVECs Ejected From the C/2011 L4 Coma[a]

	Appearance					Disappearance			Size	Phase
Clump Number	Day (3/2013)	Time (UT)	r (AU)	PA (deg)	d_1 (AU)	Day (3/2013)	Time (UT)	d_2 (d'_2) (AU)	$S \pm \Delta S$ (10^5 km)	Angle (deg)
1	11	23:29	0.300	238.8	0.076	12	07:29	0.122 (0.114)	7.51 ± 0.83	132.16–132.95
2	12	13:29	0.296	247.1	0.073	12	18:09	0.101 (0.099)	8.32 ± 0.26	133.37–133.65
3	12	21:29	0.292	251.8	0.068	13	07:29	0.145 (0.140)	9.30 ± 0.55	133.79–133.96
4	13	06:09	0.296	256.8	0.070	13	20:49	0.186 (0.182)	11.75 ± 0.67	133.96–133.64
5	13	23:29	0.305	267.7	0.070	14	15:05	0.171 (0.173)	9.97 ± 0.53	133.51–132.30
6	14	20:09	0.308	279.1	0.059	15	12:49	0.188 (0.196)	12.50 ± 0.47	131.76–129.59
7	14	22:09	0.303	280.8	0.050	15	02:49	0.079 (0.081)	9.42 ± 0.29	131.53–130.96
8	15	01:29	0.309	281.8	0.055	15	14:09	0.161 (0.167)	8.12 ± 0.29	131.13–129.39
9	15	06:09	0.313	284.0	0.054	15	12:09	0.093 (0.096)	10.01 ± 0.23	130.52–129.68
10	15	08:49	0.315	285.4	0.052	15	22:49	0.165 (0.175)	12.96 ± 0.51	130.16–128.03
11	15	12:09	0.316	287.6	0.049	16	01:29	0.137 (0.146)	6.25 ± 0.27	129.68–127.60
12	15	12:49	0.309	288.7	0.041	16	00:09	0.121 (0.129)	6.20 ± 0.29	129.59–127.82

[a]PA and r are the position angle of the ejecta and heliocentric distance at their first appearance. PA is measured counterclockwise from the solar north. Variables d_1 and d_2 are the cometocentric distances of the clumps at their appearance and disappearance, respectively. Variable d'_2 is the disappearance cometocentric distances of the clumps with respect to the comet position at their appearance. The last column provides the variation of the comet's phase angle from the appearance to disappearance of each HVEC.

resolution of the HI-2B observations. It is clear from Figure 3 and Table 1 that the number of ejecta increased after the comet crossed the ecliptic plane, particularly on 14–15 March. The dynamical evolution of the ejected clumps as observed by HI1-B is shown in Figure 4.

Figures 4a and 4b show the propagation trajectories of the HVECs as they crossed the HI1-B FOV antisunward. The clump appearance correspond to the moment when a coherent structure is distinguishable from the other structures and can be followed for several frames. Their disappearance is the moment when they can no longer be clearly discernible from background. The clump positions correspond to their approximate centers as seen in the running-difference images. They are determined interactively by hand using remapping of the images from pixel elongation into heliocentric distance and position angle. The remapping software is included in the STEREO package in the SSW tree. The error on the HVECs' positions is assumed to be equal to their respective size precision, which is a conservative approach. They follow nearly radial lines where the change of the position angle is $< 2°$ in all cases (Figure 4b). This is evidence for near-radial propagation of the HVECs with respect to the Sun. The ejecta propagation paths may bear clues to their interaction with the ambient solar wind that is presumably propagating radially in this region of the solar system.

Since the excess in white-light emission can be due to scattering by free electrons and/or dust grains, the white-light data do not directly provide insights into the composition of these clumps. These may be composed of submicron dust particles that are swept away under the influence of solar radiation pressure, the solar wind, and charging effects. They may also be composed of neutral or ionized atomic/molecular species (e.g., Na^{+0} or K^{+0}, Li^{+0} or Ca^{+0}, or Na^{+} or K^{+} alkali ions) [see *Fulle et al.*, 2007, 2013].

3.1. Clump Dynamics

Figure 4c shows the dynamical evolution of the ejected HVECs. Speeds measured at the HVECs' first detection, as estimated from the observed motion of clumps in the HI1-B images and then corrected for projection effects (i.e., $v_X / \sin\alpha$ and $v_Y / \sin\alpha$ components, where α is the phase angle of the comet) range between 200 and 400 km s^{-1}. The ejecta undergo a subsequently large acceleration, resulting in an increase of speeds up to 450–600 km s^{-1}. The bulk speed of the ejecta seem to reach a plateau at 500–600 km s^{-1}. The latter are typical values of slow to intermediate solar wind speeds. The solid gray curve in Figure 4c is a polynomial fit of all measured velocities. The dashed curves show that most of the measurements lie within the ± 100 km s^{-1} of the best fit. The ejecta acceleration is mainly in the X direction (image horizontal). Velocities in the Y direction (image vertical) remain nearly constant with the exception of ejecta in the Southern Hemisphere. Velocities in the Y direction are signed depending on the location where the clump ejection occurs (i.e., positive

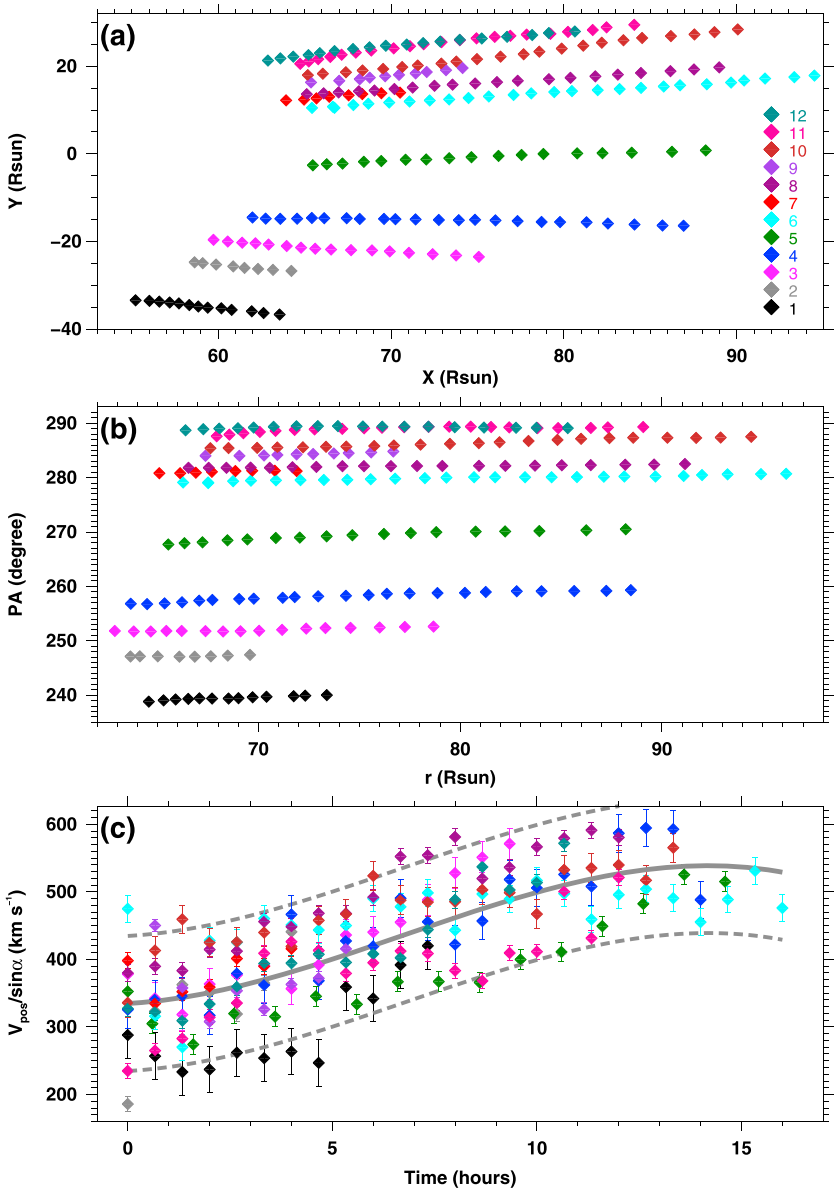

Figure 4. (a, b) Propagation paths of the 12 HVECs listed in Table 1. The symbols and the corresponding clump numbers in Table 1are shown in Figure 4a. The clump trajectories are near radially aligned as illustrated by the position angles that vary by less than 2° for all clumps. (c) Bulk velocity of the HVECs corrected for projection effects (i.e., $V_{pos}/\sin\alpha$, where V_{pos} is the plane-of-the-sky speeds of the clumps as estimated from the observed motion of clumps in the HI1-B images; α is the phase angle of the comet). The solid gray curve is the best polynomial fit of the clump propagation velocities. The dashed lines show that more than 90% of measured velocities lie within the best curve ±100 km s^{-1}. The HVECs are accelerated mainly in the radial direction from initial speed values of 200–400 km s^{-1} up to 450–600 km s^{-1} where a plateau is seemingly reached. The velocity error bars are computed using the ΔS that are assumed to be the accuracy of the HVECs' position measurements.

(negative) for clumps emitted northward (southward) of the ecliptic plane). A dynamical equilibrium seems to be reached once velocities similar to those of the local environment (i.e., the solar wind) are attained.

The inferred velocity values are much higher than the typical speeds of dust particles ejected from comets' nuclei (i.e., $<0.5-1$ km s^{-1}) [*Bobrovnikoff*, 1930; *Finson and Probstein*, 1968; *Lisse et al.*, 1998, 2004]. For a ~1 μm particle, the acceleration due to solar radiation pressure is ≈ 0.13 m s^{-2} at 0.23 AU. At this acceleration, it takes $\sim 2.7\times10^6$ s to reach velocities $v\sim350$ km s^{-1} in a distance of $\sim 2\times10^8$ km (1.4 AU). Neither of these values is in agreement with the time interval ($\sim 2\times10^4$ s) or distances ($\sim 5\times10^6$ km) seen in our SECCHI observations. Moreover, unlike the Lorentz force that results in an acceleration having a q/m dependence, the acceleration

due to solar gravity is independent of an object's mass. This is because the acceleration due to solar radiation pressure is roughly equal to $\beta\times$ the acceleration due to solar gravity, which is also mass independent. For the Mie theory

$$\beta = \frac{F_{\text{rad pressure}}}{F_{\text{gravity}}} = \frac{0.47(\mu\text{m})}{N(\text{gcm}^{-3})\,R(\mu\text{m})} \approx \frac{\text{Surface Area}}{\text{Volume}},$$

where N is the mass density of the dust particles and R is the radius. Since the observed clumps have a $\Delta V \sim 200$ km s^{-1} in about 5 h (Figure 4c), this implies an average acceleration in that time of $\sim$11.1 m s^{-2}, and thus an effective β value of 11.1/0.13 = 84.6 or higher. Except for some predictions of high β values for neutral alkali atom (due to the strong doublet transitions in Li, Na, and K) and neutral Ca, β values of cometary species do not approach these values [see *Fulle et al.*, 2013]. It is noteworthy, however, that the HI-1B transmissions for Na and K are very inefficient, only $\sim$1%. C/2011 L4 would need at least 10^{25} to 10^{26} Na atoms to show up at all in HI1-B. We also note that the photoionization lifetime of these neutral atoms is on the order of 10^4 s [*Fulle et al.*, 2007], which is long enough to stay neutral in the FOV of SECCHI. It is therefore reasonable to assume that unless some mechanism is creating large clumps of neutral alkali or Ca atoms that solar radiation pressure does not play an important role in the acceleration of the HVECs up to $\sim$200–400 km s^{-1}. The images (Figure 3) do not show evidence for size growth (i.e., cross-field diffusion) of the HVECs. This may suggest that the clumps may be composed of ionized species whose dynamics are controlled by the HMF.

Assuming that the acceleration is due solely to the Lorentz force $\vec{a} = \frac{q}{m}\vec{v}\times\vec{B}$, $v_{\text{initial}} \approx 350$ km s^{-1} (at the clump initial detection; see Figure 4c), an average solar wind magnetic field strength of $|\mathbf{B}| = 20 - 30$ nT at 0.3 AU [see *Korth et al.*, 2011] and that the accelerated species are mainly composed of ionized sodium atoms (note that strong Na emission lines have been reported by *Cochran et al.* [2013] in observations of comet C/2011 L4 from the Dunn telescope in March 2013) with $\frac{q}{m} = \frac{1.6\times10^{-19}}{23\times1.6\times10^{-27}} \approx 4.3\times10^6$ C kg^{-1} results in an acceleration $a \sim 4.5\times10^4$ m s^{-2}. This suggests that the composition of the clumps is likely not dominated by ionized species as small as single atoms.

If on the other hand the clumps are mainly composed of charged submicron dust particles with much smaller effective q/m values, we can explain the observed accelerations. Specifically, if we are observing singly charged particles, then a dust particle of mass 3×10^3 times a Na atom's mass would exhibit the observed acceleration. Such a particle would only have to be about 10 Na atoms in radius. Since real particles are just as likely to be made of rocky silicates than Na metal, or, following Yang et al.'s results, water ice, we should use the effective molecular weights for water ice (18 amu) or olivine (140 amu) to determine the minimum radius of the observed particles. In the case of water ice, a singly charged particle of $\sim$11 molecules radius ($\sim 2\times10^{-3}$ μm) will exhibit the observed acceleration; for an olivine particle, a particle of only 5 (Mg_2SiO_4) units in radius ($\sim1.5\times10^{-3}$ μm) will behave as observed. These radii increase by $q_{\text{eff}}^{0.333}$, where q_{eff} is the average charge on the grains.

We thus suggest that the HVECs are most likely clouds of ionized submicron dust grains that are carried by the solar wind under the effect of the $\mathbf{E}\times\mathbf{B}$ forces. We cannot, however, completely rule out the possibility of neutral atoms/molecules dominated clumps.

3.2. Clump-Striae Relationship

Figure 3 and the movie provided as supplementary material show that the HVECs are expelled along bright features initially elongated near radially (i.e., along the clumps' direction of propagation). These elongated structures subsequently bend backward to the comet's orbital motion. They progressively evolve into new striae in the dust tail (see Figures 3g–3l). The HVECs-striae connection is illustrated by the movie frames 18–26, 29–36, 81–96, and 109–134, where bright clumps can be seen originating from elongated structures that result subsequently in a striae. In spite of the limited extent of the observations in time and heliodistance coverage, the data may also indicate that the timing of the bright clumps and the related, newly forming striae may originate from rotational modulation of localized areas of strong outgassing occurring on the surface of the comet's main body (i.e., nucleus) as suggested by *Fulle et al.* [2013]. This phenomena is noticeable all along the comet crossing of the HI-1B FOV and may be appreciated better through animated images (see the movie provided in the supporting information). A relationship between the comet nucleus' rotation and the striae spacing is reasonable as we measure a separation between the striae on the order of 10^5 km, which at differential orbital velocities on the order of 1 to 10 km s^{-1} for the larger dust implies a time between outgassing activity maxima $\sim10^4$ to $\sim10^5$ s, or 3 to 30 h. The comet nucleus rotation is the only regularly

periodic clock in the system varying with period on the order of hours to days, and staying regular over days to weeks; the solar wind is much more stochastic on these timescales.

Although the one-to-one connection between the HVECs and striae needs to be confirmed, if this is indeed the case, it would provide new insights into the nature and formation mechanism(s) of the dust tail striae and the role of the local environment (i.e., solar wind in the present case) in the evolution and sorting of cometary dust and/or atomic/molecular species, in general. It also bears clues on activity phenomena occurring on the comet surface and the dynamics of the nucleus that are not easily accessible otherwise.

4. Discussion and Conclusions

Detailed analysis of white-light observations from STEREO/SECCHI/HI-1B show evidence for episodical, rapidly fading clumps ejected from the coma of C/2011 L4. They were initially observed on 10 March 2013, closely after C/2011 L4 entered the HI-1B FOV. These structures are easily identified in the running-difference images initially at cometocentric distances ranging from $\sim 6 \times 10^6$ km to $\sim 10^7$ km ($\sim$0.041–0.076 AU; see Table 1) from the nucleus (see Figure 1 and Table 1). They last for several hours and propagate to larger cometocentric distances ranging from 0.09 AU to 0.18 AU. They do not seem to undergo significant expansion and their sizes remain roughly constant. The number of ejecta increased after the comet crossed the ecliptic plane, particularly on 14–15 March (see Figure 3 and Table 1). The bright clumps are swept near radially in the antisunward direction regardless of their ejection times and locations along the comet's orbit. Their initial velocities range from 200 to 400 km s^{-1} and are followed by an appreciable acceleration up to velocities of 450–600 km s^{-1}, where a plateau is seemingly reached (see Figure 4). The latter values are typical of slow and intermediate solar wind speeds. A number of these ejecta could also be traced into the HI-2B FOV.

The white-light images from HI-1B do not provide direct information about the origin of the clump material. The data indicate, however, that the HVECs may originate from discrete events occurring within the coma and are likely the result of dust and gas jets on the surface of a comet's rotating nucleus. It is unlikely that they are the result of continuous processes of dust and atomic/molecular species expulsion from the nucleus surface. *Fulle et al.* [2013] reported on spectroscopic observations showing the abundance of alkali atoms sublimated from the comet's nucleus at distances beyond the water-ice sublimation zone, providing evidence for processes energetic enough to extract atomic species and dust from the nucleus.

The STEREO image morphology indicates that dust in the coma undergoes a sorting process where very small submicron particles are carried antisunward by the solar wind, while larger supramicron particles evolve to flow into the dust tail where they contribute to the formation of prominent striae. Whether the submicron particles are emitted directly from the nucleus surface or are instead the product of a subsequent dust fragmentation process that occurs at the beginning of the striae (cf. the models of *Sekanina and Farrell* [1980], *Pittichová et al.* [1997], and *Nishioka* [1998]) is not clear—although the STEREO imagery would suggest the latter as a real possibility. Since the striae are typically only seen in very dusty comets at small heliocentric distances, we can posit the existence of a population of fractal, porous dust grains in these comets held together by materials that disrupts after a period of exposure to solar radiation and the solar wind, releasing a distribution of smaller grains that go on to form the clumps and the striae. The clump particles may also be charged throughout the interaction with local environment (i.e., solar radiation and solar wind) and are then picked up by the HMF. The dynamics of the ionized species are completely controlled by the solar wind and its frozen-in magnetic field.

Two physical processes can affect the dynamics of the dusty comet ejecta:

1. *Solar radiation pressure*. It is expected that the material expelled from the comet nucleus lies within the sunward sector of the coma. Solar radiation pressure may contribute significantly (at least in the initial stages) to the acceleration of atomic/molecular species and submicron dust particles in the antisolar direction. The influence of the solar radiation pressure on dust particles larger than 1.0 μm is limited, which may explain the formation of new striae. If the ejected clumps are composed of dust grains, radiation pressure contributes to the initial size sorting of the dust expelled from the comet surface.
2. *Pickup of charged particles by the HMF*. The interaction of the ejected particles with the solar wind resulting in their pickup by the local magnetic field, which may inhibit cross-field diffusion and then the expansion of the observed structures.

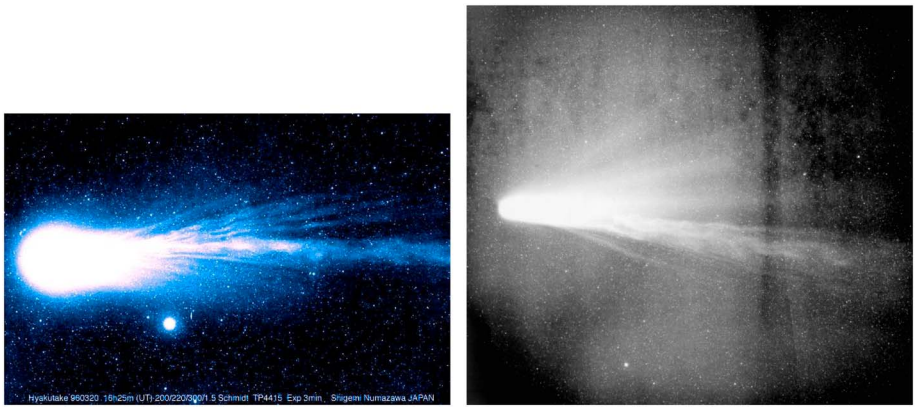

Figure 5. (left) Image of comet Hyakutake taken on 20 March 1996 by Shigemi Numazawa. The multiple clump-like features in the highly structured tail are of striking similarity to the morphology detected for comet C/2011 L4 (Pan-STARRS) by STEREO. (right) This morphology appeared also, although with much worse observing geometry, in comet 1P/Halley 1986.

Although we cannot definitively determine the composition of the ejected material, dynamics of the clump excess emission in white-light may only be attributed to (1) dusty sources via a combination of scattering by positively charged dust grains and excess free electrons due to charged neutrality in the solar wind, (2) scattering by a high beta neutral atomic species, or (3) fluorescence of an ionized species. Order of magnitude calculations show that solar radiation pressure can be ruled out as the main accelerator of dust particles and that ionized single atoms or molecules accelerate too quickly compared to observations, while dust grains micron sized or larger accelerate too slowly. Neutral Na, Li, K, or Ca atoms with $\beta > 50$ could also fit the observations. The lack of expansion of the clumps may hint that these may be composed of ionized species that cannot undergo cross-field diffusion. In the case of ionized submicron dust material, we find that an interaction with the solar wind and the HMF can cause the observed clump dynamical evolution. We thus suggest that HVECs are clouds of ionized submicron dust grains that are carried by the solar wind under the effect of the $\mathbf{E} \times \mathbf{B}$ forces. We cannot, however, completely rule out the possibility of neutral atoms/molecules dominated clumps.

Another interesting aspect of the HVECs is their apparent connection to newly forming striae in the dust tail. The data show that the HVECs move initially along and then detach from near-radial bright structures. The latter progressively bend backward to the comet's orbital motion and form new striae. This suggests that both phenomena may be the result of nucleus activity modulated by its rotation. The clump-striae relationship may provide new insights into comet's nuclei activity and the role of the local environment in the evolution and sorting of cometary ejected material. The one-to-one connection between clumps and striae needs to be confirmed, however.

The nature and composition of the ejected clumps as well as the mechanisms responsible for their acceleration may be constrained by additional observations (e.g., spectroscopic) and rigorous modeling. The detailed dynamical modeling of the structures in the C/2011 L4 tail is beyond the scope of this paper and will be studied in detail in a follow-up paper.

The STEREO observations of comet C/2011 L4 (Pan-STARRS) that we have described here are compelling. But they become more interesting when we use our identification of the clump phenomenon to search for them in other comets. The most obvious starting point for this search are in other comets known to have produced strong striae structures. Examination of the archival record shows an extremely similar coma/tail morphology for comet 1P/Halley in 1910 and 1986 (Figure 5). Clump-like structures were also seen in comet C/1995 O1 (Hale-Bopp). Not so obvious, though, were clumps in the coma/tail of comets C/2001 V1 (NEAT) as observed by SOHO or comet C/2006 P1 (McNaught) as observed from Earth, despite the latter comet displaying an extraordinary sweep of striae across many degrees of the evening twilight sky. Future models of clumps and striae will have to rate this variability into account. On the other hand, the dust and gas composition, dust size distribution, and dust/gas emission rates are known to vary significantly from comet to comet, so it may be the variation in one of these quantities (e.g., the sodium atom abundance) that controls the clump brightness.

Acknowledgments
The authors are grateful for the anonymous referees for constructive comments and suggestions. We would like to thank A. Vourlidas (JHUAPL) for helpful comments and suggestions. N.-E.R. would like to thank NASA's Solar Probe Plus mission for supporting partially the present work. G.H.J. is partially supported by the Science and Technology Facilities Council, UK. The data used in the present analysis were acquired from the Virtual Solar Observatory (VSO: http://www.virtualsolar.org) database and were processed to higher levels using the STEREO/SECCHI/HI-1 calibration procedures available on Solar Software tree (SSW: http://www.lmsal.com/solarsoft). The STEREO/SECCHI data are produced by an international consortium of the NRL (USA), LMSAL (USA), NASA-GSFC (USA), RAL (UK), University of Birmingham (UK), MPS (Germany), CSL (Belgium), IOTA (France), and IAS (France).

Larry Kepko thanks two anonymous reviewers for their assistance in evaluating this paper.

References

A'Hearn, M. F., et al. (2005), Deep impact: Excavating comet Tempel 1, *Science*, *310*, 258–264, doi:10.1126/science.1118923.
Bar-Nun, A., and D. Laufer (2003), First experimental studies of large samples of gas-laden amorphous "cometary" ices, *Icarus*, *161*, 157–163, doi:10.1016/S0019-1035(02)00016-7.
Bewsher, D., D. S. Brown, and C. J. Eyles (2012), Long-term evolution of the photometric calibration of the STEREO heliospheric imagers: I. HI-1, *Sol. Phys.*, *276*, 491–499, doi:10.1007/s11207-011-9874-7.
Bobrovnikoff, N. T. (1930), Halley's comet in 1910, *Publ. Astron. Soc. Pac.*, *42*, 309, doi:10.1086/124062.
Boehnhardt, H. (2004), Split comets, in *Comets II*, vol. 745, edited by M. C. Festou, H. U. Keller, and H. A. Weaver, pp. 301–316, Univ. of Ariz Press, Tucson.
Brandt, J. C. (1968), The physics of comet tails, *Annu. Rev. Astron. Astrophys.*, *6*, 267–286, doi:10.1146/annurev.aa.06.090168.001411.
Brownlee, D. E., et al. (2004), Surface of young Jupiter family comet 81 P/Wild 2: View from the stardust spacecraft, *Science*, *304*, 1764–1769, doi:10.1126/science.1097899.
Buffington, A., M. M. Bisi, J. M. Clover, P. P. Hick, B. V. Jackson, and T. A. Kuchar (2008), Analysis of plasma-tail motions for comets C/2001 Q4 (NEAT) and C/2002 T7 (LINEAR) using observations from SMEI, *Astrophys. J.*, *677*, 798–807, doi:10.1086/529039.
Clark, B. C., S. F. Green, T. E. Economou, S. A. Sandford, M. E. Zolensky, N. McBride, and D. E. Brownlee (2004), Release and fragmentation of aggregates to produce heterogeneous, lumpy coma streams, *J. Geophys. Res.*, *109*, E12S03, doi:10.1029/2004JE002319.
Clover, J. M., B. V. Jackson, A. Buffington, P. P. Hick, and M. M. Bisi (2010), Solar wind speed inferred from cometary plasma tails using observations from STEREO HI-1, *Astrophys. J.*, *713*, 394, doi:10.1088/0004-637X/713/1/394.
Cochran, A. L., D. H. Wooden, A. J. McKay, G. Cauzzi, K. Reardon, and G. Tozzi (2013), Spatially resolved spectroscopic observations of Na and K in the Tail of Comet C/2011 L4 (PanSTARRS), *AAS/Division for Planetary Sciences Meeting Abstracts*, *45*, 502.05.
Combi, M. R., J.-L. Bertaux, E. Quémerais, S. Ferron, J. T. T. Mäkinen, and G. Aptekar (2014), Water production in comets C/2011 l4 (Pan-STARRS) and C/2012 f6 (Lemmon) from observations with SOHO/SWAN, *Astron. J.*, *147*, 126, doi:10.1088/0004-6256/147/6/126.
Ershkovich, A. I. (1976), Solar wind interaction with the tail of comet Kohoutek, *Planet. Space Sci.*, *24*, 287–291, doi:10.1016/0032-0633(76)90025-8.
Eyles, C. J., et al. (2009), The heliospheric imagers onboard the STEREO mission, *Sol. Phys.*, *254*, 387–445, doi:10.1007/s11207-008-9299-0.
Farnham, T. L., and K. J. Meech (1994), Comparison of the plasma tails of four comets: P/Halley, Okazaki-Levy-Rudenko, Austin, and Levy, *Astrophys. J. (Supp.)*, *91*, 419–460, doi:10.1086/191943.
Finson, M. J., and R. F. Probstein (1968), A theory of dust comets: I. Model and equations, *Astrophys. J.*, *154*, 327–352, doi:10.1086/149761.
Fulle, M., F. Leblanc, R. A. Harrison, C. J. Davis, C. J. Eyles, J. P. Halain, R. A. Howard, D. Bockelée-Morvan, G. Cremonese, and T. Scarmato (2007), Discovery of the atomic iron tail of comet MCNaught using the heliospheric imager on STEREO, *Astrophys. J.*, *661*, L93–L96, doi:10.1086/518719.
Fulle, M., P. Molaro, L. Buzzi, and P. Valisa (2013), Potassium detection and lithium depletion in comets C/2011 L4 (Pan-STARRS) and C/1965 S1 (Ikeya-Seki), *Astrophys. J.*, *771*, L21, doi:10.1088/2041-8205/771/2/L21.
Glassmeier, K.-H., H. Boehnhardt, D. Koschny, E. Kührt, and I. Richter (2007), The Rosetta mission: Flying towards the origin of the solar system, *Space Sci. Rev.*, *128*, 1–21, doi:10.1007/s11214-006-9140-8.
Hill, J. R., and D. A. Mendis (1980), On the origin of striae in cometary dust tails, *Astrophys. J.*, *242*, 395–401, doi:10.1086/158472.
Howard, R. A., et al. (2008), Sun Earth Connection Coronal and Heliospheric Investigation (SECCHI), *Space Sci. Rev.*, *136*, 67–115, doi:10.1007/s11214-008-9341-4.
Jackson, B. V., A. Buffington, J. M. Clover, P. P. Hick, H.-S. Yu, and M. M. Bisi (2013), Using comet plasma tails to study the solar wind, *AIP Conf. Proc.*, *1539*, 364, doi:10.1063/1.4811062.
Jia, Y. D., C. T. Russell, L. K. Jian, W. B. Manchester, O. Cohen, A. Vourlidas, K. C. Hansen, M. R. Combi, and T. I. Gombosi (2009), Study of the 2007 April 20 CME-comet interaction event with an MHD model, *Astrophys. J.*, *696*, L56, doi:10.1088/0004-637X/696/1/L56.
Jones, G. H., and J. C. Brandt (2004), The interaction of comet 153P/Ikeya-Zhang with interplanetary coronal mass ejections: Identification of fast ICME signatures, *Geophys. Res. Lett.*, *31*, L20805, doi:10.1029/2004GL021166.
Jones, G. H., J. S. Morrill, D. Hammer, C. M. Lisse, T. L. Farnham, and G. R. Lawrence (2004), Comet C/2002 V1 (NEAT)—Evidence of solar wind effects on a comet's ion and dust tails at 0.1 AU. American Astronomical Society, DPS meeting 36, 21.02, Bulletin of the American Astronomical Society, vol. 36, p.1117.
Kaiser, M. L., T. A. Kucera, J. M. Davila, O. C. St. Cyr, M. Guhathakurta, and E. Christian (2008), The STEREO mission: An introduction, *Space Sci. Rev.*, *136*, 5–16, doi:10.1007/s11214-007-9277-0.
Keller, H. U., et al. (1986), First Halley multicolour camera imaging results from Giotto, *Nature*, *321*, 320–326, doi:10.1038/321320a0.
Keller, H. U., W. A. Delamere, H. J. Reitsema, W. F. Huebner, and H. U. Schmidt (1987), Comet P/Halley's nucleus and its activity, *Astron. Astrophys.*, *187*, 807–823.
Kimura, H., H. Okamoto, and T. Mukai (2002), Radiation pressure and the Poynting-Robertson effect for fluffy dust particles, *Icarus*, *157*, 349–361, doi:10.1006/icar.2002.6849.
Konno, I., W. F. Huebner, and D. C. Boice (1990), A hydrodynamic model of dusty gas flows in comet Comae with dust fragmentation. *Lunar Planet. Sci. Conf.*, *21*, 653.
Konno, I., W. F. Huebner, and D. C. Boice (1993), A model of dust fragmentation in near-nucleus jet-like features on comet P/Halley, *Icarus*, *101*, 84–94, doi:10.1006/icar.1993.1008.
Korth, H., B. J. Anderson, T. H. Zurbuchen, J. A. Slavin, S. Perri, S. A. Boardsen, D. N. Baker, S. C. Solomon, and R. L. McNutt (2011), The interplanetary magnetic field environment at Mercury's orbit, *Planet. Space Sci.*, *59*, 2075–2085, doi:10.1016/j.pss.2010.10.014.
Kramer, E. A., Y. R. Fernandez, C. M. Lisse, M. S. P. Kelley, and L. M. Woodney (2014), A dynamical analysis of the dust tail of comet C/1995 O1 (Hale-Bopp) at high heliocentric distances, *Icarus*, *236*, 136–145, doi:10.1016/j.icarus.2014.03.033.
Królikowska, M., P. A. Dybczyński, and G. Sitarski (2012), Different dynamical histories for comets C/2001 Q4 and C/2002 T7?, *Astron. Astrophys.*, *544*, A119, doi:10.1051/0004-6361/201219408.
Lee, S., et al. (2014), Sub-millimeter observation of water vapor at 557 GHz in comet C/2002 T7 (LINEAR), *Icarus*, *239*, 141–153, doi:10.1016/j.icarus.2014.05.004.
Lisse, C. M., M. F. A'Hearn, M. G. Hauser, T. Kelsall, D. J. Lien, S. H. Moseley, W. T. Reach, and R. F. Silverberg (1998), Infrared Observations of comets by COBE, *Astrophys. J.*, *496*, 971, doi:10.1086/305397.
Lisse, C. M., et al. (2004), A tale of two very different comets: ISO and MSX measurements of dust emission from 126P/IRAS (1996) and 2P/Encke (1997), *Icarus*, *171*, 444–462, doi:10.1016/j.icarus.2004.05.015.
Meech, K. J., and J. Svoren (2004), Using cometary activity to trace the physical and chemical evolution of cometary nuclei, in *Comets II*, vol. 745, edited by M. C. Festou, H. U. Keller, and H. A. Weaver, pp. 317–335, Univ. of Ariz Press, Tucson.

Mendis, D. A., E. J. Smith, B. T. Tsurutani, J. A. Slavin, D. E. Jones, and G. L. Siscoe (1986), Comet-solar wind interaction: Dynamical length scales and models, *Geophys. Res. Lett.*, *13*, 239–242, doi:10.1029/GL013i003p00239.

Mendis, D. A., and M. Horányi (1991), Dust-plasma interactions in the cometary environment, in *Cometary Plasma Processes (A92-10001 01-90)*, pp. 17–25, AGU, Washington, D. C.

Mendis, D. A., and M. Horányi (2013), Dusty plasma effects in comets: Expectations for Rosetta, *Rev. Geophys.*, *51*, 53–75, doi:10.1002/rog.20005.

Nishioka, K., and J.-I. Watanabe (1990), Finite lifetime fragment model for synchronic band formation in dust tails of comets, *Icarus*, *87*, 403–411, doi:10.1016/0019-1035(90)90143-W.

Nishioka, K. (1998), Finite lifetime fragment model 2 for synchronic band formation in dust tails of comets, *Icarus*, *134*, 24–34, doi:10.1006/icar.1998.5935.

Notesco, G., A. Bar-Nun, and T. Owen (2003), Gas trapping in water ice at very low deposition rates and implications for comets, *Icarus*, *162*, 183–189, doi:10.1016/S0019-1035(02)00059-3.

Notni, P., and W. Thaenert (1988), The striae in the dust tails of great comets—A comparison to various theories, *Astron. Nachr.*, *309*, 133–146.

Oppenheim, A. V., R. W. Schafer, and T. G. Jr. Stockham (1968), Nonlinear filtering of multiplied and convolved signals, *Proc. IEEE*, *56*(8), 1264–1291, doi:10.1109/TAU.1968.1161990.

Prialnik, D. (1992), Crystallization, sublimation, and gas release in the interior of a porous comet nucleus, *Astrophys. J.*, *388*, 196–202, doi:10.1086/171143.

Pittichová, J., Z. Sekanina, K. Birkle, H. Boehnhardt, D. Engels, and P. Keller (1997), An early investigation of the striated tail of comet Hale-Bopp (C/1995 O1), *Earth Moon Planets*, *78*, 329–338, doi:10.1023/A:1006242209416.

Russell, C. T., J. G. Luhmann, R. C. Elphic, and M. Neugebauer (1982), Solar wind interaction with comets—Lessons from Venus. IAU Colloq. 61: Comet Discoveries, Statistics, and Observational Selection, pp. 561–587.

Sekanina, Z., and J. A. Farrell (1980), The striated dust tail of comet West 1976 VI as a particle fragmentation phenomenon, *Astron. J.*, *85*, 1538–1554, doi:10.1086/112831.

Sekanina, Z., and J. A. Farrell (1982), Two dust populations of particle fragments in the striated tail of comet MRKOS 1957 V, *Astron. J.*, *87*, 1836–1853, doi:10.1086/113274.

Sekanina, Z., D. E. Brownlee, T. E. Economou, A. J. Tuzzolino, and S. F. Green (2004), Modeling the nucleus and jets of comet 81P/Wild 2 based on the stardust encounter data, *Science*, *304*, 1769–1774, doi:10.1126/science.1098388.

Sekanina, Z. (2007), Dust jets, outbursts, and fragmentation of comets, in *Instruments, Methods, and Missions for Astrobiology X*, edited by R. B. Hoover et al., *Proc. SPIE, 6694*, San Diego, Calif.

Socker, D. G., R. A. Howard, C. M. Korendyke, G. M. Simnett, and D. F. Webb (2000), *NASA Solar Terrestrial Relations Observatory (STEREO) mission heliospheric imager*, in *Instrumentation for UV/EUV Astronomy and Solar Missions*, edited by S. Fineschi et al., *Proc. SPIE, 4139*, 284–293, Bibliographic Code: 2000SPIE.4139..284S.

Soderblom, L. A., et al. (2002a), Observations of comet 19P/Borrelly by the miniature integrated camera and spectrometer aboard deep space 1, *Science*, *296*, 1087–1091, doi:10.1126/science.1069527.

Soderblom, L. A., et al. (2002b), Encounter with comet 19P/Borrelly: Results from the Deep Space 1 Miniature Integrated Camera and Spectrometer, *Lunar Planet. Sci. Conf.*, *33*, 1256.

Tuzzolino, A. J., et al. (2004), Dust measurements in the coma of comet 81P/Wild 2 by the Dust Flux Monitor Instrument, *Science*, *304*, 1776–1780, doi:10.1126/science.1098759.

Wainscoat, R., M. Micheli, L. Wells, R. Holmes, S. Foglia, T. Vorobjov, G. Sostero, E. Guido, H. Sato, and G. V. Williams (2011), Comet C/2011 L4 (Pan-STARRS). IAU circ., 9215, 1.

Whipple, F. L. (1951), A comet model: II. Physical relations for comets and meteors, *Astrophys. J.*, *113*, 464–474, doi:10.1086/145416.

Yang, B., J. Keane, K. Meech, T. Owen, and R. Wainscoat (2014), Multi-wavelength observations of comet C/2011 L4 (Pan-STARRS), *Astrophys. J.*, *784*, L23, doi:10.1088/2041-8205/784/2/L23.

Yelle, R. V., L. A. Soderblom, and J. R. Jokipii (2004), Formation of jets in comet 19P/Borrelly by subsurface geysers, *Icarus*, *167*, 30–36, doi:10.1016/j.icarus.2003.08.020.